# Supplementary Material
# Infrared up-conversion imaging in nonlinear metasurfaces

**Rocio Camacho-Morales**[a*]**, Davide Rocco**[b]**, Lei Xu**[a,c,d]**, Valerio Flavio Gili**[e,f]**, Nikolay Dimitrov**[g]**, Lyubomir Stoyanov**[g]**, Zhonghua Ma**[a]**, Andrei Komar**[a]**, Mykhaylo Lysevych**[a]**, Fouad Karouta**[a]**, Alexander Dreischuh**[g]**, Hark Hoe Tan**[a]**, Giuseppe Leo**[e]**, Costantino De Angelis**[b]**, Chennupati Jagadish**[a]**, Andrey E. Miroshnichenko**[c]**, Mohsen Rahmani**[a,d]**, Dragomir N. Neshev**[a]

[a]ARC Centre of Excellence for Transformative Meta-Optical Systems (TMOS), Department of Electronic Materials Engineering, Research School of Physics, The Australian National University, Canberra, ACT 2601, Australia
[b]Department of Information Engineering, University of Brescia, Via Branze 38, 25123 Brescia, Italy
[c]School of Engineering and Information Technology, University of New South Wales, Canberra, ACT 2600, Australia
[d]Advanced Optics and Photonics Laboratory, Department of Engineering, School of Science and Technology, Nottingham Trent University, Nottingham, NG11 8NS, UK
[e]Matériaux et Phénomènes Quantiques, Université Paris Diderot, F-75013 Paris, France
[f]Institute of Applied Physics, Abbe Center of Photonics, Friedrich Schiller University Jena, 07745 Jena, Germany
[g]Department of Quantum Electronics, Faculty of Physics, Sofia University, 5 J. Bourchier Blvd., Sofia 1164, Bulgaria

## S1 Numerical calculations

The linear and nonlinear optical response of the (110) GaAs metasurface is numerically modeled by using the Finite Element Method in Comsol Multiphysics. The nonlinear response is obtained in a two-step approach. First, we calculate the nonlinear polarization response of the metasurface $\mathbf{P}(\omega_3)$ resulting from the incident pump and signal frequency beams. Then, we employ the nonlinear polarization as the source to calculate the SFG, through the induced nonlinear current $\mathbf{J}(\omega_3)$. We define the $i$-th component of the nonlinear electric polarization vector at the angular frequency $\omega_3$ as

$$P_i(\omega_3) = \epsilon_0 \chi^{(2)} [E_j(\omega_1)E_k(\omega_2) + E_k(\omega_1)E_j(\omega_2)], \tag{1}$$

with $i \neq j \neq i$ due to the zinc-blende crystal structure of GaAs. Here $\epsilon_0$ is the vacuum permittivity, $E_j(\omega_1)$ is the $j$-th component of the electric field at the angular frequency $\omega_1$ and $E_k(\omega_2)$ is the $k$-th component of the electric field at the angular frequency $\omega_2$. The angular frequencies $\omega_1$, $\omega_2$ and $\omega_3$ correspond to the wavelength of the signal at 1530 nm, the pump at 860 nm, and the SFG at 550 nm, respectively. The GaAs metasurface is simulated by implementing Floquet boundary conditions to mimic an infinite 2D periodic structure.

Figure S1 shows the calculated reflection of our (110) GaAs metasurface ($P = 750$ nm, $r = 225$ nm and $h = 400$ nm), as a function of incident wavelength. As shown in Figure S1, at long wavelengths the reflection spectrum has mainly electric and magnetic dipole contributions, while for shorter wavelengths the reflection spectrum has additional contributions from electric and magnetic quadrupole modes. Thus, at the incident IR signal beam ($\lambda$=1530 nm) the main contributions are electric and magnetic dipole modes. On the other hand, at the incident pump beam ($\lambda$=860 nm), the resonant behavior of the metasurface is explained by the combination of dipoles and quadrupole modes of electric and magnetic nature.

When considering the lattice effects of the GaAs metasurface, the sum-frequency emission will be shaped into different diffraction orders, depending on the periodicity $P$ of the metasurface. Figure S4 shows the sum-frequency diffraction coefficients of our GaAs metasurface generated by
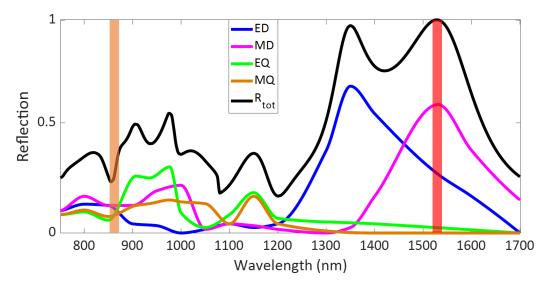
**Fig S1** Calculated total reflection spectrum (black solid line, $R_{tot}$) and multipolar decomposition of GaAs metasurface, as a function of incident wavelength. The multipolar decomposition shows the main contributions of the reflection spectrum, namely electric dipole (ED), magnetic dipole (MD), electric quadrupole (EQ) and magnetic quadruple (MQ). The orange and red vertical lines indicate the wavelength of the pump (860 nm) and signal (1530 nm) beams, respectively.

the simultaneous incidence of an IR signal beam at 1530 nm and a pump at 860 nm. The SFG diffraction coefficients are calculated by performing the Fourier transform of the sum-frequency near field in both directions, backward and forward. As indicated by the color intensity scale in Figure S4a and b, in each direction the strongest SFG emission corresponds to the zero-th diffraction order. In both directions, the first diffraction orders in the *x*- and *y*-directions have lower intensity than the zero-th diffraction order. Overall, the forward SFG intensity is stronger than the backward SFG. In our metasurface, there are no second diffraction orders for the sum-frequency emission.
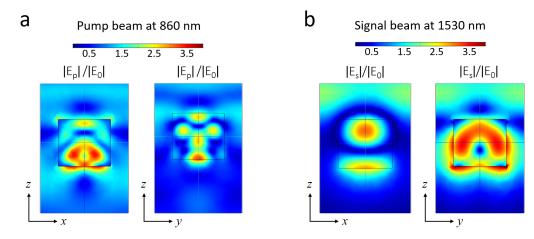


**Fig S2** Calculated modulus of electric field distribution through the center of GaAs metasurface unitary cell (*r*=225 nm, *h*=400 nm) at an incident wavelength of (a) 860 and (b) 1530 nm.

SFG emission at 550 nm

x 10⁻³



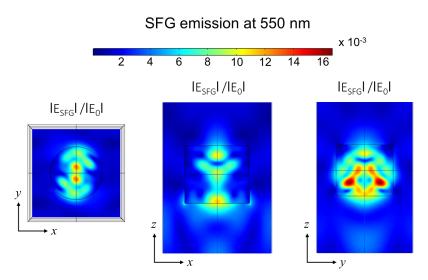$|E_{SFG}|/|E_0|$  $|E_{SFG}|/|E_0|$  $|E_{SFG}|/|E_0|$

**Fig S3** Calculated modulus of the sum-frequency electric field distribution, across the center of the *xy*-, *xz*- and *yz*-plane of GaAs metasurface unitary cell ($r = 225$ nm, $h = 400$ nm). The SFG field is generated at 550 nm by the simultaneous incidence of pump and signal beams at 860 and 1530 nm, respectively. Here $E_0$ refers to the amplitude of the incident pump beam.
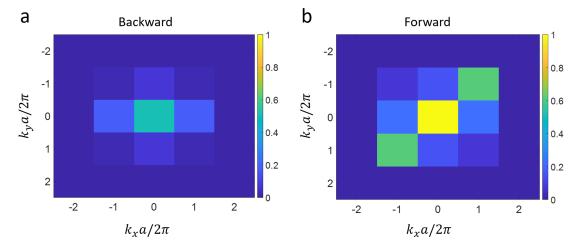
a Backward        b Forward



**Fig S4** Far-field diffraction distribution of SFG calculated in the (a) backward and (b) forward direction to the GaAs metasurface, when simultaneously excited by a pump beam at 860 nm and a signal beam at 1530 nm. The color scale of SFG intensity is shown at the right side of each plot.

3

## S2 Experimental setup and measurements

The schematic of the optical system used to characterize the nonlinear optical response of the GaAs metasurface is shown in Figure S5. A Ti:Sapphire laser (Coherent, Chameleon Ultra II) pumps an optical parametric oscillator cavity (Coherent, Chameleon Compact OPO), which provides a short-wave IR signal beam and an unconverted beam with the same wavelength as the Ti:Sapphire pump. Therefore, at the output of the OPO cavity two beams with the same polarization (horizontal) and repetition rate (80 MHz), but different wavelength, are used as the signal and pump excitation beams. The polarization angle of the signal and pump beams can be controlled separately by two half-wave plates, *HWP* (Thorlabs, AHWP10M-980 and AHWP05M-1600). Temporal synchronization of the signal and pump pulsed laser beams is achieved by tuning an optical delay line which consists of two mirrors sitting at about 90 degrees to each other, mounted in a travel translation stage (Thorlabs, PT1/M). The signal and pump beams are spatially combined by a dichroic mirror, *DM* (Thorlabs, Low-GDD Ultrafast Mirror) and then focused at the same position on the GaAs metasurface, *MS* by a plano-convex lens, *L1* with $f$=50 mm. The nonlinear radiation generated by the GaAs metasurface, together with the transmitted excitation beams, are collected by a 100X objective lens with a NA of 0.5 (Mitutoyo, Plan Apo NIR Infinity). At the back aperture of the objective lens, two short-pass filters, *Fs* with cut-off wavelengths of 600 and 800 nm (Thorlabs, FESH0600 and FESH0800) are used to filter-out the transmitted excitation beams. The transmitted nonlinear emissions are either focused by a plano-convex lens, *L2* with $f$=75 mm in the CCD of a camera (Starlight Xpress, SXVR-H9) or coupled by a fiber collimator lens, *L3* to an optical fiber connected to a visible spectrometer (Ocean Optics, QE65000).
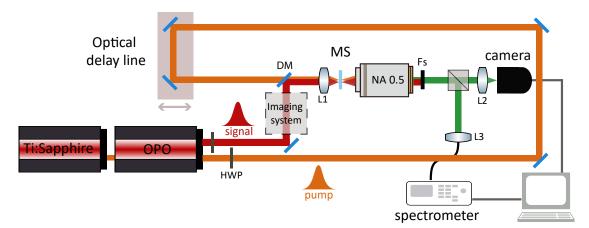


**Fig S5** Schematic of optical system used to study the nonlinear emissions generated by (110) GaAs metasurface. The schematic shows the optical path of the signal and pump pulsed laser beams employed to excite the metasurface and generate sum-frequency emission at green wavelengths. The IR up-conversion imaging is performed by using the imaging system in the IR signal beam. In the schematic, the focused pump and signal beams are not spatially overlapped only for visualization purposes.

Figures S6a and b show typical temporal spectra of the Ti:Sapphire laser at 860 nm, and the OPO cavity at 1520 nm, measured with a spectral autocorrelator (Swamp Optics, Grenouille). The spectra were measured at the output of the OPO cavity (see Figure S5), before the half-wave plates. Material dispersion effects can be induced in the excitation beams due to the glass of the different optical components (*e.g.* focusing lens and half-wave plates). These effects, however, are not

significant for the duration of the pulsed excitation beams used in this work, therefore they were neglected. Therefore, the duration of the pulses at the metasurface plane can be taken from the duration measured at the output of the OPO cavity.
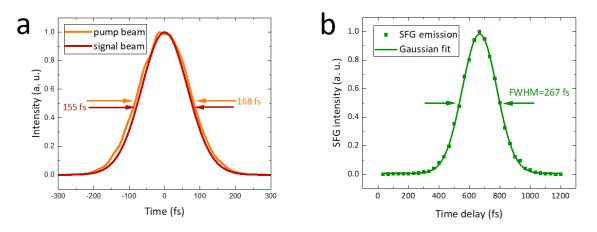


**Fig S6** Cross correlation of the pump pulsed laser beam with the signal pulsed laser beam. (a) The duration of the signal and pump laser beams was directly measured, giving a pulse-width of 155 and 168 fs, respectively. (b) The duration of the SFG emission was measured using an optical delay line, giving a pulse-width of 267 fs.

Figure S7 shows a schematic of the imaging system built to encode the information of a target in the IR signal beam. The imaging system consists of a Keplerian telescope that projects the real image of the target onto the metasurface plane as explined below. First, a resolution target (Thorlabs, R1L3S5P) is placed at the focal distance of a plano-convex lens, $L$ with $f = 100$ mm. The transversal position of the target (across the $xy$-plane) is controlled by a translation mount (Thorlabs, XYF1/M). After the target, a 5X objective lens with NA of 0.14 (Mitutoyo, Plan Apo NIR Infinity) is used to collect the signal beam. The objective lens is fixed at its working distance, $WD$ from the target which results in a confocal configuration. Through this imaging system, a collimated IR signal beam containing the real image of the target is obtained. The collimated signal beam is focused on the metasurface plane by a lens (see $L1$ in Figure S5) projecting a real IR image of the target onto the metasurface plane.

Fourier imaging of the $SHG_{2\omega p}$ and SFG emissions was performed as shown in Figure S8. The measurements were performed by placing a flip plano-convex lens ($f$=50 mm) after the collecting objective lens to project the Fourier plane on the CCD camera. In Figure S8 only the zero and first diffraction orders are observed, while the higher diffraction orders emitted by the metasurface are not collected by the optical system (see FigureS4). In the case of the SFG emission, the first diffraction orders are emitted close to the maximum collection angle of the objective lens, hence, only a small portion of these diffracted emissions is observed.
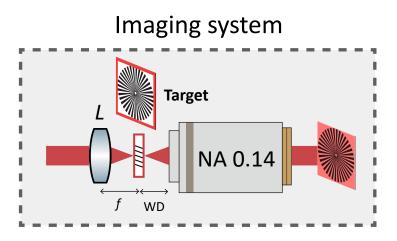
# Imaging system



**Fig S7** Schematic of imaging system employed to encode real image of a Siemens star target in the IR signal beam (and subsequently in the SFG beam). The system consists of a lens (L) with $f = 100$ mm and an objective lens with NA of 0.14, placed in a confocal configuration.
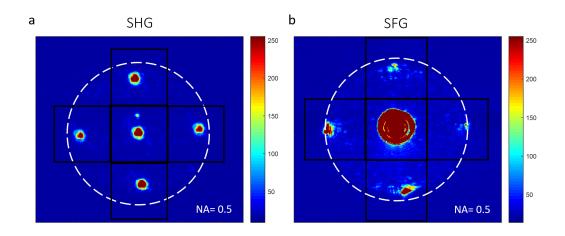


**Fig S8** Fourier plane images of (a) SHG and (b) SFG emissions generated by the metasurface. The dashed white circle indicates the maximum angular filed of view due to the NA of the collecting objective lens. The black squares denote the different diffraction orders of the nonlinear emissions. The intensities of the images are not comparable to each other since they were taken with different camera integration time.

*S2.1 SFG efficiency*

| | P$^{ave}$(mW) | $\tau$ (fs) | P$^{peak}$(KW) | I(GW/cm$^2$) |
|---|---|---|---|---|
| Pump beam | 16.4 | 168 | 1.235 | 0.78 |
| Signal beam | 16.8 | 155 | 1.354 | 0.38 |

**Table S1** Experimental values of pump and signal beams employed in the calculation of the SFG efficiency.

$$\eta = P_{SFG}/P_s^{ave} = 5 \times 10^{-8} \tag{2}$$

$$\eta_{norm} = \eta/P_p^{ave} = 3.6 \times 10^{-6}\,[W^{-1}] \tag{3}$$